INT. J. HYPERTHERMIA, 1994, VOL. 10, NO. 4, 517–536

Temperature-dependent versus constant-rate blood perfusion modelling in ferromagnetic thermoseed hyperthermia: results with a model of the human prostate

D. T. TOMPKINS†‡, R. VANDERBY†§, S. A. KLEIN†,
W. A. BECKMAN†, R. A. STEEVES‡, D. M. FRYE‡*
and B. R. PALIWAL‡*

†Departments of Mechanical Engineering, ‡Human Oncology, and *Medical Physics, University of Wisconsin–Madison, Madison, WI 53792, USA

(*Received 2 April 1993; revised 12 October 1993; accepted 28 October 1993*)

Finite-element solutions to the Pennes bioheat equation are obtained with a model of a tumour-containing, human prostate and surrounding normal tissues. Simulations of ferromagnetic hyperthermia treatments are conducted on the tissue model in which the prostate is implanted with an irregularly spaced array of thermoseeds. Several combinations of thermoseed temperatures with different Curie points are investigated. Non-uniform, constant-rate blood perfusion models are studied and compared with temperature-dependent descriptions of blood perfusion. Blood perfusions in the temperature-dependent models initially increase with tissue temperature and then decrease at higher temperatures. Simulations with temperature-dependent versus constant-rate blood perfusion models reveal significant differences in temperature distributions in and surrounding the tumour-containing prostate. Results from the simulations include differences (between temperature-dependent and constant-rate models) in (1) the percentage of normal tissue volume and tumour volume at temperatures $>42°C$, and (2) temperature descriptors in the tumour (subscript t) and normal (subscript n) tissues including $T_{max,t}$, $T_{min,t}$ and $T_{max,n}$. Isotherms and grey-scale contours in the tumour and surrounding normal tissues are presented for four simulations that model a combination of high-temperature thermoseeds. Several simulations show that $T_{min,t}$ is between 1·7 and 2·6°C higher and $T_{max,n}$ is between 2·1 and 3·3°C higher with a temperature-dependent versus a comparable constant-rate blood perfusion model. The same simulations reveal that the percentages of tumour volume at temperatures $>42°C$ are between 0 and 68% higher with the temperature-dependent versus the constant-rate perfusion model over all seed combinations studied. In summary, a numerical method is presented which makes it possible to investigate temperature-dependent, continuous functions of blood perfusion in simulations of hyperthermia treatments. Simulations with this numerical method reveal that the use of constant-rate instead of temperature-dependent blood perfusion models can be a conservative approach in treatment planning of ferromagnetic hyperthermia.

Key words: Ferromagnetic hyperthermia, thermal modelling, temperature-dependent blood perfusion, thermoseeds, treatment planning

1. Introduction

Ferromagnetic hyperthermia utilizes cylindrically-shaped, metallic alloys, called thermoseeds, that are placed surgically into tumours and, if desired, surrounding normal tissues. A coil placed around the patient produces an electromagnetic field that causes eddy-current heating of the thermoseeds. Tissues near the thermoseeds are then heated via thermal conduction. Ferromagnetic hyperthermia has been investigated in both

§Author for correspondence.

theoretical and/or experimental studies (Atkinson *et al.* 1984, Brezovich *et al.* 1984, 1990, Matloubieh *et al.* 1984, Stauffer *et al.* 1984a,b, Lilly *et al.* 1985, Kobayashi *et al.* 1986, Mechling and Strohbehn 1986, Chen *et al.* 1988, 1990–1992, Vanderby *et al.* 1988, Partington *et al.* 1989, Chin and Stauffer 1991, Haider *et al.* 1991, 1993, Tompkins *et al.* 1994).

Several studies that predict temperatures in tissue models assumed to be undergoing a ferromagnetic hyperthermia treatment have used constant-rate blood perfusion models (Atkinson *et al.* 1984, Brezovich *et al.* 1984, Matloubieh *et al.* 1984, Stauffer *et al.* 1984a,b, Mechling and Strohbehn 1986, Vanderby *et al.* 1988, Chen *et al.* 1990–1992, Chin and Stauffer 1991, Haider *et al.* 1993, Tompkins *et al.* 1994). Methods for estimating the complete temperature field from measured data have been studied (Clegg *et al.* 1985, Clegg and Roemer 1989, Liauh *et al.* 1991, Liauh and Roemer 1993a,b). In reconstructing the temperature field, these methods typically assume a uniform blood perfusion in each of several zones throughout the tissue model, and are, therefore, discontinuous at the interfaces between each zone. Thus treatment simulations of ferromagnetic hyperthermia are subject to a constant-rate blood perfusion assumption either throughout each tissue model or in finite-sized zones within tissue models.

It has been reported that blood perfusion depends on temperature especially in normal muscle and skin tissues (Song *et al.* 1984). Because previous studies (Atkinson *et al.* 1984, Brezovich *et al.* 1984, Matloubieh *et al.* 1984, Stauffer *et al.* 1984a,b, Mechling and Strohbehn 1986, Vanderby *et al.* 1988, Chen *et al.* 1990–1992, Chin and Stauffer 1991, Haider *et al.* 1993, Tompkins *et al.* 1994) have used a constant-rate blood perfusion assumption, the treatment implications of temperature-dependent blood perfusion, as predicted by thermal modelling, is not well understood. Therefore the goal of this paper is to investigate the influence of temperature-dependent versus constant-rate blood perfusion models. Simulations are performed on a model of a tumour-containing, human prostate implanted with an array of ferromagnetic thermoseeds with various Curie-point temperatures. Results from this comparative study should be useful in treatment simulations of ferromagnetic hyperthermia and other conductive and nonconductive hyperthermia treatment modalities.

2. Numerical approach

2.1. *Thermoseed and catheter models and numerical solution technique*

The mathematical model used in the simulations is the steady-state form of the bioheat equation (Pennes 1948)

$$k\nabla^2 T - Wc_b(T - T_b) + q_a = 0, \tag{1}$$

where k is the thermal conductivity (W/m/°C); W is the mass flow rate of blood per unit volume of tissue (kg/s/m^3) which is equal to $\rho_t \rho_b m$ where ρ_t is the density of tissue (kg/m^3), ρ_b is the density of blood (kg/m^3), and m is the volumetric flow rate of blood per unit mass of tissue (m^3/s/kg); c_b is the specific heat of blood (J/kg/°C); q_a is the energy absorption rate per unit volume of the seeds (W/m^3); T is the scalar temperature (°C); T_b is the blood temperature (°C); and ∇^2 is the Laplacian operator. A discussion on the formulation and limitations of the bioheat transfer equation can be found elsewhere (Roemer 1988).

The thermoseeds are cylindrically-shaped, Ni–Cu alloys with a diameter ($=2a$) of 0·9 mm (Brezovich *et al.* 1984). The power absorption of a thermoseed per unit length, P (W/m), when aligned parallel to the axial direction of a ferromagnetic coil is given by (Davies and Simpson 1979, Brezovich *et al.* 1984, Haider *et al.* 1991)

$$P' = \frac{\pi x H_0^2}{\sigma} \frac{ber(x)ber'(x)+bei(x)bei'(x)}{ber^2(x)+bei^2(x)}, \quad (2)$$

where H_0 is the amplitude of the magnetic field (A/m), x is the induction number and equal to $a\sqrt{(\omega\sigma\mu)}$ and is dimensionless; ω is equal to $2\pi f$ (1/s); σ is the electrical conductivity of the thermoseed (1/Ω/m); μ is the magnetic permeability of the thermoseed (tesla-m/A); f is the frequency of the magnetic field (Hz); *ber* and *bei* are Kelvin functions (Abramowitz and Stegun 1964); and *ber'* and *bei'* are first derivatives of Kelvin functions (Abramowitz and Stegun 1964). The simulations that follow are performed for a ferromagnetic hyperthermia treatment where the operating frequency is 90 kHz. At this frequency, absorption of electromagnetic energy by tissue is negligible. The permeability (μ) and magnetization of Ni–Cu thermoseeds depend on temperature in the hyperthermia treatment range. Thus the temperature-dependent permeability and magnetization as previously obtained (Brezovich *et al.* 1984, Figure 3) are used to determine the power absorption (P') of the thermoseed models within this study.

Heat-transfer models of catheters and self-regulating thermoseeds with operating temperatures of 48·1, 54·1 and 60·1°C (i.e. Curie points of 53, 57·6 and 62·6°C, respectively) are used in the simulations (Tompkins 1992, Tompkins *et al.* 1994). These thermoseeds were investigated because clinical experience, phantom and animal experiments and computer simulations suggest that these provide sufficient heating power for effective treatments. The thermoseed and catheter models are devoid of blood perfusion (Table 1). The catheter model has a conductivity of 0·34 W/m/°C (Clay Adams Co. 1991), and the conductivity of the seed model is assumed to be infinite (Tompkins 1992, Tompkins *et al.* 1994). Thermoseeds are modelled as sources of energy whose temperatures (T_s) depend on the power absorbed ($q_a = P'/A$, where A is the cross-sectional area of the seed) (Figure 1). An S-dimensional Newton-Raphson technique (Shoup 1979), where S is the total number of thermoseeds, is implemented into the numerical solution algorithm to iteratively determine the temperature of each thermoseed for the power absorbed (Tompkins 1992, Tompkins *et al.* 1994).

Since the tissue models and thermoseed locations studied in this paper are unsymmetrical, the finite element method, rather than an analytical approach, is used to solve for T in equation (1). Triangular-shaped finite elements, over which the temperature

Table 1. Tissue/material properties

Tissue/material type	Thermal conductivity, k (W/m/°C)	Volumetric blood flow, m (m^3/s/kg)	Tissue density, ρ_t (kg/m^3)	Blood perfusion, W (kg/s/m^3)
Bladder* (empty)	0·64	†	1080	†
Rectum*	0·64	0	–	–
Bone	1·16 (1)	$1{\cdot}12\times10^{-7}$ (5)	1500 (1)	0·177
Fat	0·19 (2)	$3{\cdot}07\times10^{-7}$ (6)	850 (1)	0·276
Muscle	0·64 (3)	†	1080 (1)	†
Tumour core*	0·64	†	1080	†
Tumour periphery*	0·64	†	1080	†
Catheter	0·34 (4)	0	–	–
Thermoseed	assumed infinite (7)	0	–	–

*Assumed to have the properties of muscle tissue.
1, Gordon *et al.* 1976; 2, Cooper and Trezek 1971; 3, Nevins and Darwish 1970; 4, Clay Adams Co. 1991; 5, Root 1963; 6, Nielsen 1972; and 7, Tompkins *et al.* 1994.
†See Table 2.

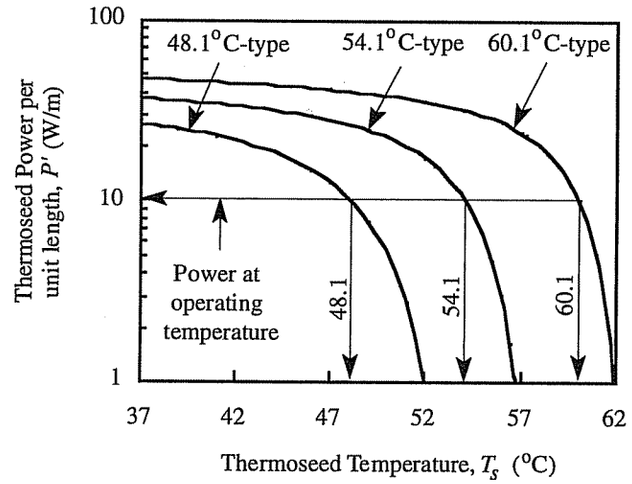

Figure 1. Power per unit length (P') absorbed by a self-regulating thermoseed as a function of temperature (T_s). A (reference) power of 10 W/m is used to define the *operating* temperatures. The curves for thermoseeds with operating temperatures of 48·1, 54·1 and 60·1 °C are generated from theory (equation 2). The Curie points for 48·1, 54·1 and 60·1 °C-type Ni–Cu thermoseeds are about 53, 57·6 and 62·6 °C (Tompkins *et al.* 1994).

distribution is assumed to be linear, are used as a basis in the finite element equations (Myers 1987, Tompkins 1992). The finite element equations are developed in a general form so that temperature-dependent properties can be studied (Tompkins 1992). The numerical solutions are obtained with a general-purpose, finite-element computer program called FEHT (pronounced 'feet') (Klein *et al.* 1988–94). FEHT can determine the temperature distribution in tissue models that have constant, spatially, temperature and/or time-dependent thermophysical properties and energy generation and temperature- and/or time-dependent boundary conditions.

2.2. *Human prostate model*

Simulations are performed on the cross-section shown in Figure 2, a slice near the midpoint of the prostate proceeding in a cephalic to caudal direction. The cross-section in Figure 2 is selected because it contains the largest cross-sectional area of the prostate. In addition, it has been shown that two-dimensional (versus three-dimensional) modelling of ferromagnetic hyperthermia tissue models is adequate so long as the cross-section which is modelled is further than 10 mm from the ends of the thermoseeds (Chin and Stauffer 1991). Also, two-dimensional modelling is justified so long as the thermoseeds are longer than 30 mm and the cross-section is the centrally-located plane (Chen *et al.* 1991). The cross-section in Figure 2 and thermoseed lengths (>50 mm) used in this study satisfy these requirements.

In Figure 2, the contour line closest to the centre of the image defines the tumour-containing prostate. It is assumed that the entire prostate is infiltrated with tumour cells. Earlier studies and clinical experience have shown that often the inner core of the tumour is a tough, fibrous tissue and may have a blood perfusion that differs vastly from that in the outer periphery of the tumour (Falk 1978). Thus the tumour is modelled as two distinct regions consisting of an inner core and an outer periphery (Figure 3). The boundary between the core and periphery is chosen arbitrarily.

The circular-shaped contour anterior to the prostate (or above the prostate in Figure 2) defines the bladder. The rectum is the contour line posterior to the prostate (or below the prostate in Figure 2). During the hyperthermia treatment, the bladder will drain due to gravity and will be smaller and have no urine inside. Thus the bladder region is modelled as a region of muscle tissue.

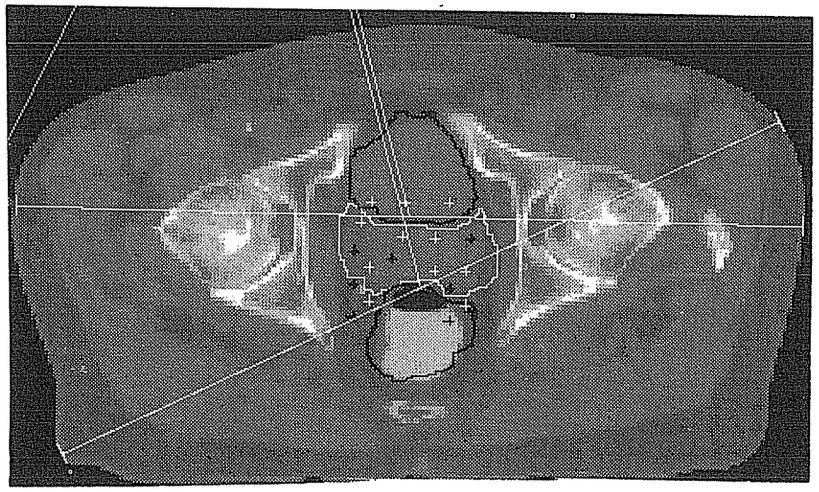

Figure 2. Image of a transverse plane near the mid-plane of the prostate. The contour nearest the centre of the image is the tumour-containing prostate. The contour anterior to (or above) the prostate defines the (empty) bladder. The contour posterior to (or below) the prostate defines the rectum. The cross-hairs are locations of catheters. The white-coloured lines are length scales.

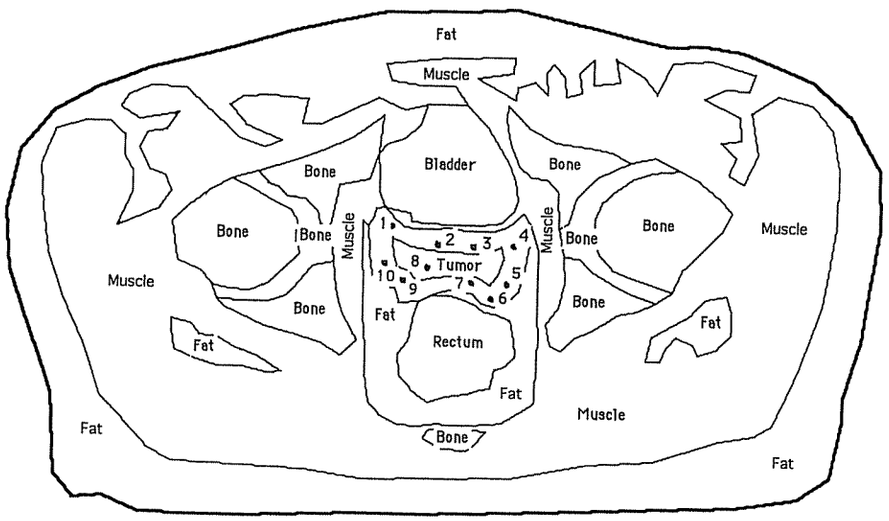

Figure 3. Contours of tissue models and the locations of thermoseed and catheter models used in simulations. The tumour (i.e. prostate) is modelled as two distinct regions consisting of an inner core and an outer periphery. The black-coloured circles 1–5, 7, 9 and 10 in the outer periphery of the tumour are the locations of the thermoseed-catheter models. Circles 6 and 8 are the locations of the catheters used for temperature measurements.

The black-coloured area in the upper region of the rectum in Figure 2 is the location of an air pocket in the rectum (i.e. gas). This air pocket is small relative to the cross-sectional area of the rectum and other tissues. The air pocket is about 10 mm in length (Tompkins 1992). In the simulations, the air pocket is assumed to be rectum and will have thermal properties identical to those of the rectum. (By modelling the air pocket as rectal material, the predicted temperature distributions will be lower than they would have been had the air pocket been modelled as a distinct region. In other words, air pockets behave thermally as insulators.)

The cross-hairs in Figure 2 are locations of 19 catheters. The catheter locations were chosen previously by medical physicists and radiation oncologists to obtain an adequate isodose distribution of ionizing radiation emanating from iridium-192 seeds in the prostate. Ten of the catheters are located within the prostate and nine are located within the surrounding normal tissues. Of the catheters in the normal tissues, three are in the bladder and six are located in the rectum and surrounding fatty tissue which is posterior to the prostate. Usually at least two catheters are used for measuring temperatures during the hyperthermia treatment. One of these two catheters is located typically near the centre of the prostate, while the other is in the prostate and located near the boundary of the prostate and normal tissues. The maximum number of catheters, therefore, which can be loaded with thermoseeds is 17. In the simulations, however, the nine catheters in the normal tissues are not loaded with thermoseeds. Thus it is possible to study the temperature distribution produced by thermoseeds located only within the prostate. In the remainder of this paper, the tumour-containing prostate is referred to simply as the tumour.

The locations of the eight thermoseed and catheter (0·35-mm wall) models (Tompkins *et al.* 1994) are the black-coloured circles 1–5, 7, 9 and 10 in Figure 3. Models of the two catheters, used for monitoring temperatures during the treatment, are shown by circle 6 in the tumour periphery and circle 8 in the tumour core and are modelled as thermoseeds without energy absorption (i.e. $P'=0$). The complete finite element mesh of the tissue model and thermoseeds is shown in Figure 4. A mesh of 1904 elements satisfied the requirement for convergence and accuracy of the numerical solution (Tompkins 1992). The outer edge of the tissue system is modelled with a convection boundary ($h=5$ W/m^2/°C (Incropera and DeWitt 1990) and $T_{amb}=25$°C). All tissues are perfused by blood at T_b (=37°C).

2.3. *Thermal properties and temperature-dependent blood perfusion in tissue models*

The thermal conductivities of tumours have been measured previously. Jain *et al.* (1979) have measured the thermal conductivity of a tumour of mammary origin (Walker 256 carcinoma) using a non-invasive probe technique, while Bowman (1980) has measured thermal conductivity of tumours using invasive probe techniques. The numerical values of thermal conductivity and density in the tissue models are shown in Table 1. The thermal conductivities and densities of the tissues are assumed to be independent of temperature over the hyperthermic temperature range and are considered uniform throughout each tissue type. The thermal conductivity ($k=0{\cdot}64$ W/m/°C) and density ($\rho_t=1080$ kg/m^3) of the tumour, bladder and rectum are assumed equal to that of muscle†.

Blood perfusion rates can depend on temperature over the hyperthermic temperature range. Experiments with muscle tissues of mice have revealed large increases in blood perfusion rates with increasing temperature (Song *et al.* 1984). Song *et al.* (1984) have

†A thermal conductivity of 0·64 W/m/°C for the tumour is close to that for squamous cell of the lung ($k=0{\cdot}67$ W/m/°C) (Jain 1985).

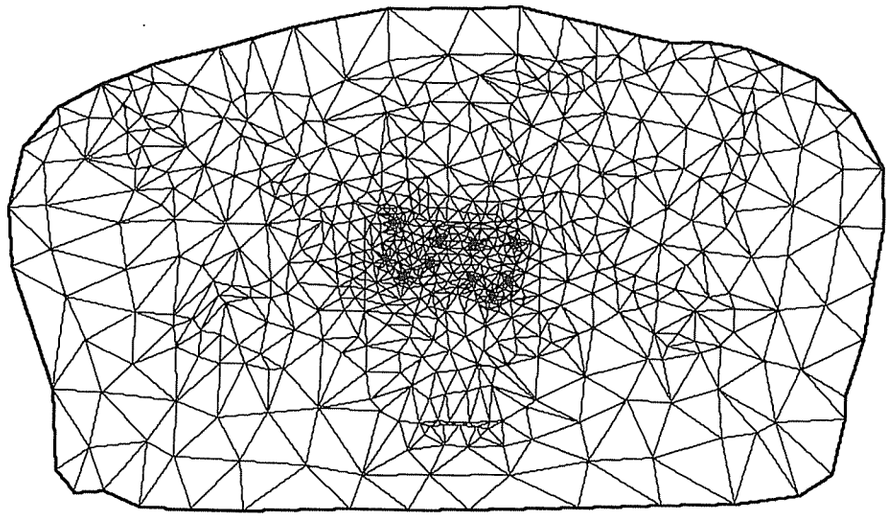

Figure 4. Finite element mesh of the tissue model shown in Figure 3. The mesh contains eight thermoseed and catheter models and two catheter models for thermometry. Finite elements are concentrated near each catheter model resulting in darkened areas. There is a convection boundary condition on the outer surface with $h=5$ W/m^2/°C (Incropera and DeWitt 1990) and $T_{amb}=25$°C: $-kA(\partial T/\partial n)|_{surface}=hA(T-T_{amb})$. The thermoseeds have an energy absorption rate per unit length (P') at their boundary as given by equation 2.

plotted the relative‡ change in blood perfusion in the muscle of rats and a scatter plot of blood perfusions in animal tumours after heating for 30–40 min at various temperatures (Figure 5). The relative changes in blood perfusion for muscle and tumour tissues are transformed into blood perfusion with dimensional units by assuming that the volumetric flow rate of blood per unit mass (m) in muscle before heating is $4{\cdot}5\times10^{-7}$ m^3/s/kg (Lassen *et al.* 1964). The blood perfusion rate, W, is determined by multiplying m by the density of muscle tissue and the density of blood ($\rho_b=1060$ kg/m^3). Similar calculations are performed using m and ρ_t to determine blood perfusion (W) for bone and fat tissues (Table 1).

Models of temperature-dependent blood perfusion in the muscle and tumour are obtained from approximations of the data in Figure 5. The core of a tumour is generally believed to be a necrotic region and thus to have a low rate of blood perfusion. Since the periphery of a tumour usually has more blood vessels than the core, the tumour periphery is generally considered to have a higher rate of perfusion than that in the tumour core (Falk 1978). Thus the temperature-dependent perfusion model for the core of the tumour is obtained by approximating the lower edge of the shaded region in Figure 5 and is shown in Figure 6b. The temperature-dependent, low-rate blood perfusion model of the tumour periphery is obtained by approximating the upper edge of the shaded region in Figure 5 and is shown in Figure 6c. The temperature-dependent perfusion model for normal muscle tissue and the temperature-dependent, moderate-rate blood perfusion model of the tumour periphery are determined by approximating the curve for muscle tissue in Figure 5 as shown in Figure 6a. Because of limited blood perfusion data at high temperatures (Song *et al.* 1984), the

‡The relative change in blood flow is the ratio of blood flow at elevated temperatures to the blood flow before heating.

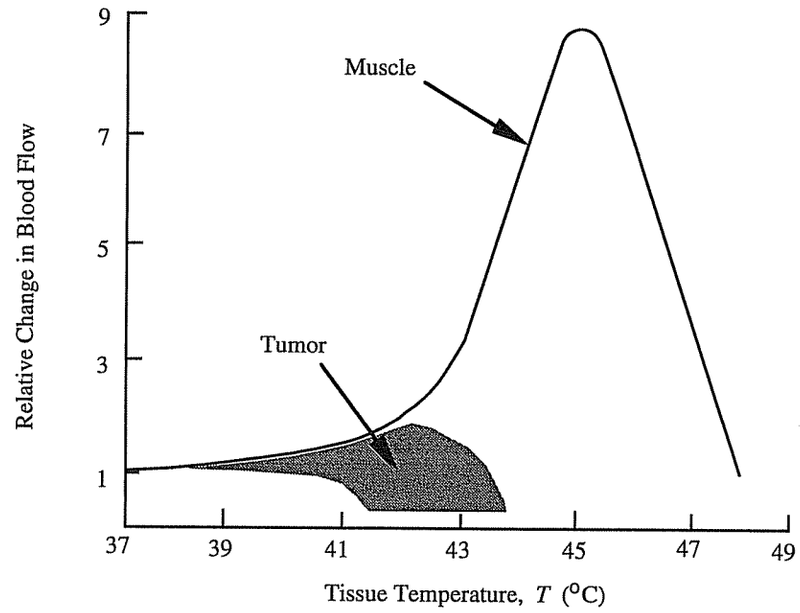

Figure 5. Temperature-dependent changes in the relative blood perfusion rates for muscle and animal tumours (reprinted from Song *et al.* 1984, Figure 3).

tissue models assume a constant rate for W at temperatures >52, 42 and 44°C as shown in Figure 6a, b and c respectively. The numerical values of the blood perfusion in the tumour core and periphery are within the range of previously measured blood perfusions in animal and human tumours (Jain 1985).

The data in Figure 6a–c are approximated by curve fits. Blood perfusion for muscle tissue is obtained by determining the maximum of two curve fits. Blood perfusion for the tumour is obtained by determining the maximum of one curve fit and a constant. The expressions for evaluating W are shown above Figure 6a–c. These expressions are used in an algorithm within the finite element solution technique to evaluate local blood perfusion as a function of temperature (Klein *et al.* 1988–94, Tompkins 1992). Within the algorithm blood perfusions are specified with initial values. Next the column vector of unknown temperatures of all finite element nodes is solved using direct techniques. Then blood perfusion values are recomputed with the known nodal temperatures. Again the nodal temperatures are redetermined. This iterative process continues until each nodal temperature between successive iterations differs by no more than 10^{-3}°C. (Thus in simulations with temperature-dependent perfusion there are two separate iterations occurring simultaneously: one to determine thermoseed temperatures as a function of the power absorbed and one to determine the local blood perfusion rate.)

2.4. *Simulations*

Simulations are performed with four blood perfusion models. Models 1 and 2 assume that blood perfusion is independent of temperature, while blood perfusions in models 3 and 4 are temperature-dependent (Table 2). Descriptions of the blood perfusion models are:

Blood perfusion model 1

Blood perfusion in normal muscle tissue is constant and nine times higher than

that in the tumour and is equal to the maximum of the curve in Figure 6a (W=4·64 kg/s/m^3).

Blood perfusion model 2

Investigates the effect of uniformly perfused muscle tissue and tumour periphery. Blood perfusion in the tumour periphery is constant (W=4·64 kg/s/m^3) and assumed equal to that in normal muscle tissue.

Blood perfusion model 3

Models for the blood perfusion in muscle tissue, the tumour core and the tumour periphery are shown in Figure 6a,b and c, respectively. The tumour periphery has a low-rate blood perfusion model (Figure 6c).

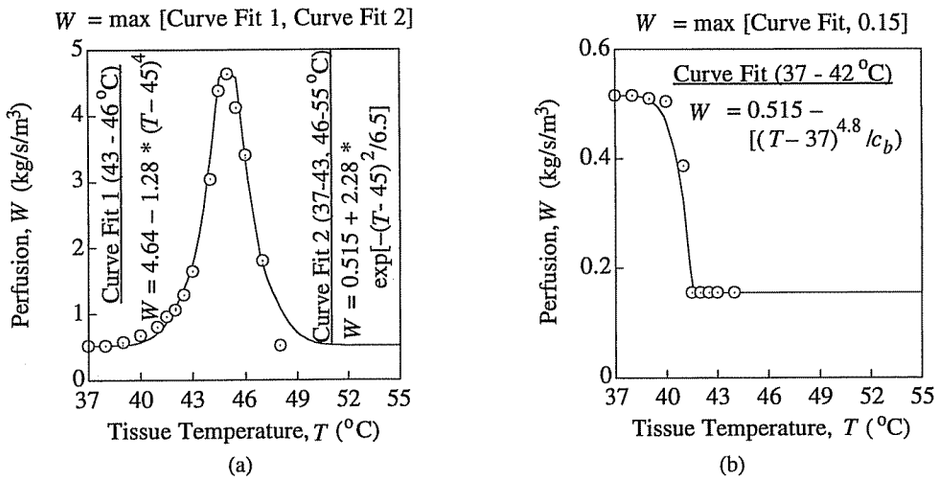

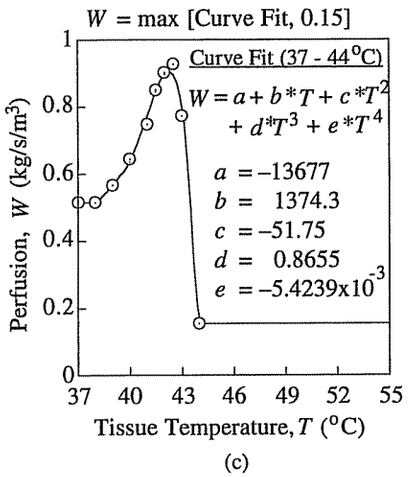

Figure 6. Models of temperature-dependent, blood perfusion for (a) muscle tissue and moderate-rate perfusion in the tumour periphery (b) the tumour core and (c) low-rate perfusion in the tumour periphery. The circles are data from the curves in Figure 5 and the solid lines are approximations of that data. Blood perfusion is obtained by determining the maximum of (a) two curve fits or (b and c) one curve fit and a constant as shown above each figure.

Table 2. Tumour and normal-muscle blood perfusion models (blood perfusions in bone and fat are given in Table 1)

Blood perfusion model	Temperature dependent?	Blood perfusion descriptors					
		Volumetric blood flow, m ($m^3/s/kg$)			Blood perfusion, W ($kg/s/m^3$)		
		Tumour core	Tumour periphery	Normal muscle	Tumour core	Tumour periphery	Normal muscle
1	No	$4{\cdot}5\times10^{-7}$	$4{\cdot}5\times10^{-7}$	$4{\cdot}05\times10^{-6}$	0·515	0·515	4·64
2	No	$4{\cdot}5\times10^{-7}$	$4{\cdot}05\times10^{-6}$	$4{\cdot}05\times10^{-6}$	0·515	4·64	4·64
3	Yes	–	–	–	‡	§	†
4	Yes	–	–	–	‡	†	†

See Figure 6: †, a; ‡, b; and §, c.

Table 3. Thermoseed combinations

Thermoseed combination	Thermoseed locations*							
	1	2	3	4	5	7	9	10
	Thermoseed type (i.e. thermoseed operating temperature; Figure 1)							
1	48·1	48·1	48·1	48·1	48·1	48·1	48·1	48·1
2	54·1	48·1	48·1	54·1	54·1	48·1	54·1	48·1
3	Mean temperature of seed combination no. 2							
4	54·1	54·1	54·1	54·1	54·1	54·1	54·1	54·1
5	60·1	54·1	54·1	60·1	60·1	54·1	60·1	54·1
6	Mean temperature of seed combination no. 5							
7	60·1	60·1	60·1	60·1	60·1	60·1	60·1	60·1

*Refer to Figure 3 for thermoseed location.

Blood perfusion model 4

Models for the blood perfusion in muscle, the tumour core and the tumour periphery are shown in Figure 6a, b and c respectively. The tumour periphery has a moderate-rate blood perfusion model and is identical to that of the normal muscle tissue (Figure 6a).

Results from simulations with blood perfusion models 3 and 4 are compared with those of models 1 and 2, respectively. Thus it will be possible to compare the effect of temperature-dependent versus constant, moderate-rate blood perfusion in normal muscle tissue (models 3 and 1, respectively) and temperature-dependent versus constant, moderate-rate perfusion in normal muscle tissue and the tumour periphery (models 4 and 2, respectively).

Simulations are performed with seven combinations of thermoseeds (Table 3). Combinations 1, 4 and 7 contain thermoseed models with operating temperatures of 48·1, 54·1 and 60·1°C, respectively. Combination 2 is considered a differentially-loaded design because it contains thermoseeds with different operating (or Curie point) temperatures. Combination 2 contains four 48·1°C-type and four 54·1°C-type thermoseeds. The four 54·1°C-type thermoseeds in combination 2 are placed in catheters near the four corners of the tumour periphery (locations 1, 4, 5 and 9 in Figure 3). (Placing high-temperature versus low-temperature seeds in the corners of the tumour may increase temperatures in the tumour periphery.) Combination 5 is another differentially-loaded design which has four 54·1°C-type and four 60·1°C-type thermoseeds. Combinations 3 and 6 are studied to compare the temperature distributions from simulations with thermoseeds at one temperature (the mean temperature of thermoseeds in combinations 2 and 5, respectively) to those from combinations 2 and 5.

3. Results

3.1. *Non-similar blood perfusion models in normal muscle tissue and tumour periphery*

Temperature distributions from simulations with temperature-dependent blood perfusion model 3 are compared with those of constant-rate blood perfusion model 1. The temperature descriptors in the tumour and normal tissues are higher with the temperature-dependent model than with the constant-rate blood perfusion model (Figure 7c). The maximum tumour temperature, $T_{max,t}$, is between 1·2 and 1·7°C higher with the temperature-dependent blood perfusion model over all seed combinations. The minimum tumour temperature, $T_{min,t}$, is between 1·9 and 2·7°C higher and the maximum normal tissue temperature,

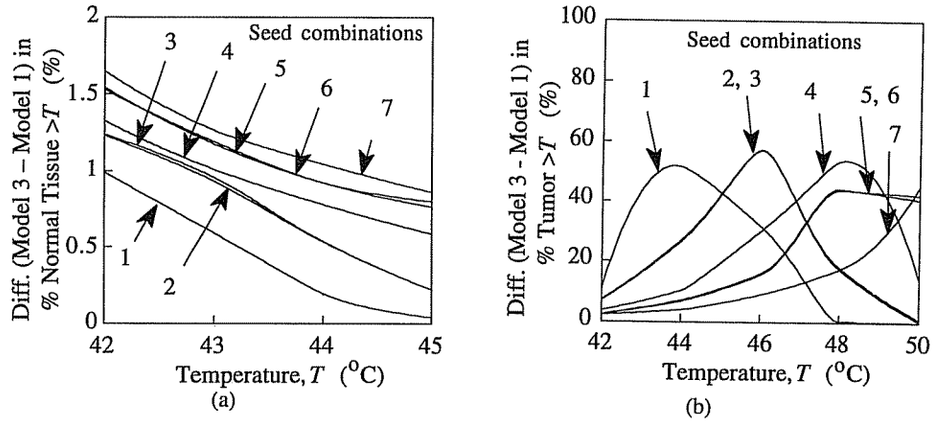

Thermoseed Combination	Temperature Difference (°C) between Blood Perfusion Models (3 – 1)		
	$T_{max,t}$	$T_{min,t}$	$T_{max,n}$
1	1.3	1.9	1.6
2	1.2	2.3	1.7
3	1.2	2.2	1.6
4	1.4	2.4	1.9
5	1.4	2.6	2.1
6	1.4	2.5	2.2
7	1.7	2.7	2.4

(c)

Figure 7. Simulation results with temperature-dependent blood perfusion model 3 versus constant-rate perfusion model 1. Results are presented as (a) differences (model 3–model 1) in the percentage of the entire normal tissue volume at temperatures >42°C, (b) differences in the percentage of tumour volume at temperatures >42°C, and (c) differences in $T_{max,t}$, $T_{min,t}$ and $T_{max,n}$. Seed combinations 1–7 are labelled in (a) and (b).

$T_{max,n}$, is between 1·6 and 2·4°C higher with the temperature-dependent blood perfusion model.

Differences in the percentage of the entire normal tissue volume at temperatures above 42°C are between 0·1 and 1·6% higher with the temperature-dependent versus the constant-rate blood perfusion model over all seed combinations (Figure 7a). Differences in the percentage of tumour volume at temperatures >42°C are between 0 and about 60% higher with the temperature-dependent perfusion model (Figure 7b).

Isotherms and grey-scale contours in and near the tumour from simulations with seed combination 7 and with the constant-rate and temperature-dependent blood perfusion models are shown in Figure 8. Larger fractions of the tumour and surrounding normal tissues are at higher temperatures with the temperature-dependent perfusion model.

3.2. *Similar blood perfusion models in normal muscle tissue and tumour periphery*

Temperature distributions from simulations with temperature-dependent blood perfusion model 4 are compared with those of constant-rate blood perfusion model 2. The temperature descriptors in the tumour and normal tissues are higher with the temperature-dependent blood perfusion model than with the constant-rate blood perfusion model (Figure 9c). $T_{max,t}$ is between 1·3 and 3·5°C higher with the temperature-dependent blood perfusion

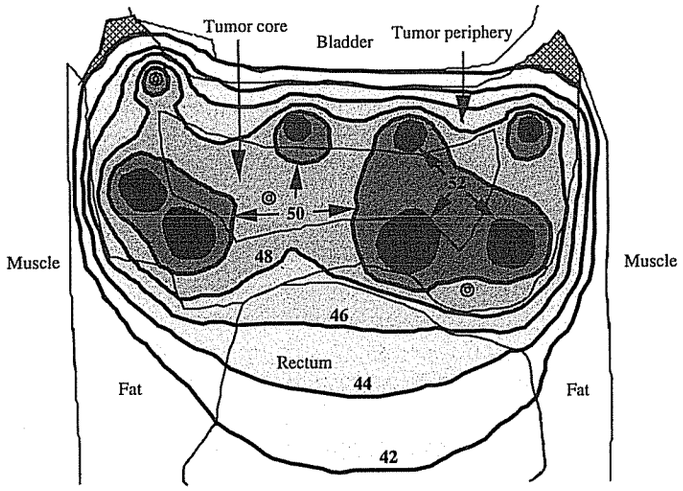

(a) Constant-rate blood perfusion model 1

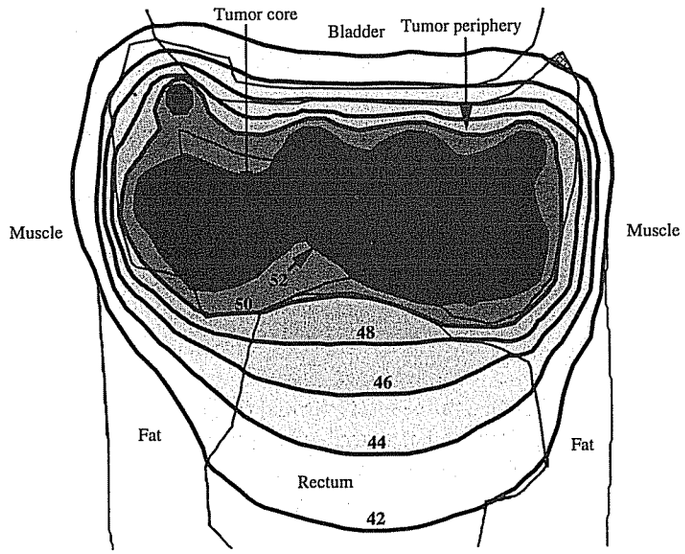

(b) Temperature-dependent blood perfusion model 3

Figure 8. Isotherms (°C) and grey-scale contours in and near the tumour from simulations with (a) constant-rate blood perfusion model 1 and (b) temperature-dependent perfusion model 3. The simulations were performed with a combination of 60·1°C-type thermoseeds (combination 7). Thermoseed and catheter models are shown by several sets of concentric circles. Temperatures of the eight thermoseeds vary between (a) 57·9 and 59·5°C and (b) 58·7 and 60·3°C. Tumour volume outside the 42°C isotherm is shown with cross-hatched shading.

model over all seed combinations. Likewise, $T_{min,t}$ is between 1·7 and 2·6°C higher and $T_{max,n}$ is between 2·1 and 3·3°C higher with the temperature-dependent blood perfusion model.

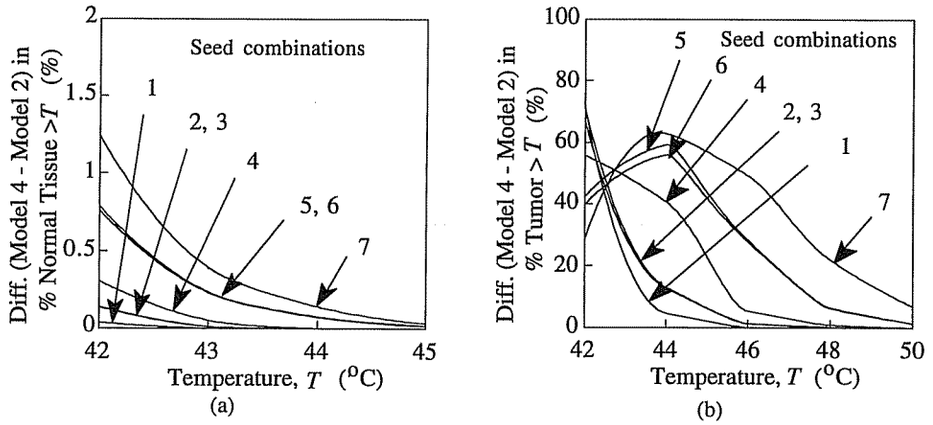

Thermoseed Combination	Temperature Difference (°C) between Blood Perfusion Models (4 – 2)		
	$T_{max,t}$	$T_{min,t}$	$T_{max,n}$
1	1.4	1.7	2.1
2	1.3	1.9	2.3
3	2.7	2.1	2.1
4	1.6	2.0	2.2
5	2.1	2.3	3.3
6	3.5	2.3	2.8
7	2.5	2.6	2.5

(c)

Figure 9. Simulation results with temperature-dependent blood perfusion model 4 versus constant-rate perfusion model 2. Results are presented as (a) differences (model 4–model 2) in the percentage of the entire normal tissue volume at temperatures $>42°C$, (b) differences in the percentage of tumour volume at temperatures $>42°C$, and (c) differences in $T_{max,t}$, $T_{min,t}$ and $T_{max,n}$. Seed combinations 1–7 are labelled in (a) and (b).

Differences in the percentage of the entire normal tissue volume at temperatures above 42 °C are between 0 and 1·25% higher with the temperature-dependent model versus the constant-rate blood perfusion model over all seed combinations (Figure 9a). Differences in the percentage of tumour volume at temperatures $>42°C$ are between 0 and 68% higher with the temperature-dependent blood perfusion model (Figure 9b).

Isotherms and grey-scale contours in and near the tumour from simulations with seed combination 7 and with the constant-rate and temperature-dependent blood perfusion models are shown in Figure 10. Significantly larger fractions of the tumour and surrounding normal tissues are at higher temperatures with the temperature-dependent perfusion model.

4. Discussion

This paper investigated the influence of temperature-dependent versus constant-rate blood perfusion models on temperature distributions produced by an interstitial array of ferromagnetic thermoseeds in a model of a tumour-containing, human prostate. The theoretical relationship to determine the power absorption of thermoseeds per unit length (equation 2) has been compared with experimental (calorimetry) data and shown to be accurate at relatively high temperatures (Brezovich *et al.* 1984). In fact the discrepancy between the theoretical and experimental data was shown to become negligible as the Curie

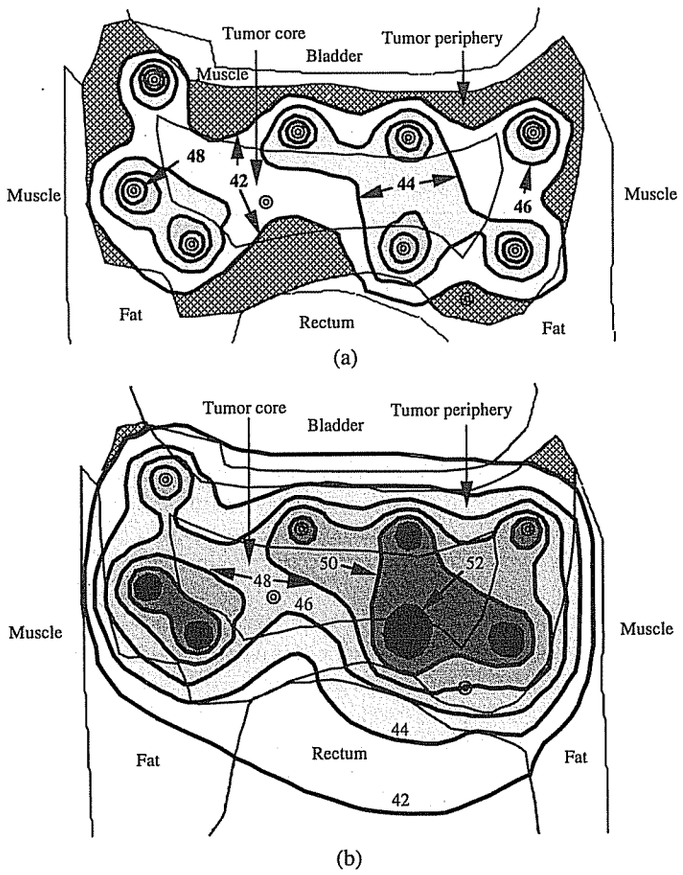

Figure 10. Isotherms (°C) and grey-scale contours in and near the tumour from simulations with (a) constant-rate blood perfusion model 2 and (b) temperature-dependent perfusion model 4. The simulations were performed with a combination of 60·1°C-type thermoseeds (combination 7). Thermoseed and catheter models are shown by several sets of concentric circles. Temperatures of the eight thermoseeds vary between (a) 56·8 and 57·4°C and (b) 57·7 and 60·0°C. Tumour volume outside the 42°C isotherm is shown with cross-hatched shading.

point is approached (Brezovich *et al.* 1984, Figure 5). Other investigators have also been successful with equation (2) in predicting the power absorption of thermoseeds (Haider *et al.* 1991).

There are, at least, two indicators that can be used to determine if the tumour periphery is heated to higher temperatures than that in surrounding normal tissues. One method is by retrospective observation of the predicted temperature contours (Figures 8 and 10). The *relative tissue perfusion* in the tumour periphery and surrounding normal muscle and fat tissues is another indicator (Song *et al.* 1984). The tissue perfusion ratio, *TPR*, is the ratio of tissue perfusion in tumour periphery to the tissue perfusion in normal muscle (or fat) tissue. Smaller tissue perfusion ratios coincide with better preferential heating of the tumour periphery. Table 4 displays *TPR*s for all four blood perfusion models at 37°C, models 1 and 3 at 48°C†, and models 2 and 4 at 43°C†. The *TPR*s for models 1 and 3 are nearly the same for muscle tissue at 48°C. The *TPR* for fat is, however, about 3·3

Table 4. Tissue perfusion ratios

Ratio of tissue types	Tissue perfusion ratio, *TPR*				
	37°C	48°C		43°C	
	All models	Model 1	Model 3	Model 2	Model 4
Tumour periphery: muscle	1	0·11	0·14	1	1
Tumour periphery: fat	1·86	1·86	0·56	16·8	6·32

times higher for model 1 than for model 3. Therefore in simulations with temperature-dependent blood perfusion (model 3), the tumour periphery is heated better preferentially than in those using a constant-rate blood perfusion model (model 1). The *TPR* for fat is about 2·7 times higher for blood perfusion model 2 than for model 4. Thus in simulations with temperature-dependent blood perfusion (model 4), the tumour periphery is heated better preferentially than in those using a constant-rate blood perfusion model (model 2). Since the blood perfusion in fat is constant in these simulations, the *TPR*s for fat might have been different if a temperature-dependent perfusion model had been used for fat. However, since adipose tissue is generally not well perfused, it is likely that the variation in blood perfusion in fat over the hyperthermic temperature range is small, especially compared with that of normal muscle tissue.

It has been stated that the periphery of a thermoseed array may be a likely site for placing thermoseeds with higher Curie temperatures to increase temperatures in the periphery of a tumour (Mechling and Strohbehn 1986, Stauffer 1990, Tompkins *et al.* 1994). Examination of Figures 7 and 9 reveal that the temperature distribution in the tumour and surrounding normal tissues from simulations with combinations of differentially-loaded thermoseeds (2 and 5) and arrays with thermoseeds at uniform temperatures (3 and 6) are similar. In addition, the isotherms in the tumour and normal tissues from simulations with (differentially-loaded) combination 5 are quite similar to those of (uniformly-loaded) combination 6 (unpublished data, Tompkins 1992, Figure 7.24). Thus using warmer seeds near the four corners of the thermoseed array had a small effect on increasing temperatures in the tumour periphery above that obtained with thermoseeds at a uniform temperature. This statement is, however, by no means general. After all, in this study the warmer thermoseeds in the differentially-loaded arrays are higher in temperature than the cooler thermoseeds by 6°C in operating temperature (Table 3). It is possible that temperatures in the tumour periphery could be increased by using even warmer (>6°C) thermoseeds in the corners of the thermoseed array.

The blood perfusion in tumours at temperatures between 37 and 50°C is not known very well but is generally believed to depend on the type, age, and size of the tumour and the local temperature (Song *et al.* 1984). In the simulations, the temperature-dependent blood perfusion models of the tumour-containing prostate are assumed equal to those in animal tumours such as the Walker carcinoma 256, Yoshida sarcoma, BA-1112 Rhabdomyosarcoma, and squamous carcinoma, among others (Song *et al.* 1984). Temperature-dependent blood perfusion in an adenocarcinoma, which is the most common type of tumour in the prostate (DeVita *et al.* 1985), is, however, not among the data points in the scatter plot in Figure 5. The low-rate, temperature-dependent blood perfusion model in the tumour periphery approximates the upper edge of measured blood perfusion in

†The 48 and 43°C isotherms enclose significant fractions ($\geq 0{\cdot}5$) of the tumour in simulations with models 1 and 3 and models 2 and 4, respectively (Figures 8 and 10). Thus *TPR*s are evaluated at 48 and 43°C.

tumours. However, it is possible that the blood perfusion in the periphery of neoplastic tissues is equal to or greater than that in surrounding normal tissues (Song *et al.* 1984). In the presence of moderate to high-rate blood perfusion and efficient heat dissipation, heat damage in the periphery of a tumour can be difficult to achieve. Thus simulations with the moderate-rate, temperature-dependent blood perfusion model in the tumour periphery were investigated. Two blood perfusion models of tumour tissue assumed a constant rate for W between 44 and 55°C for tumour tissue (Figure 6b and c). Blood perfusions in the 44–55°C temperature range are extrapolated from perfusion rates at 44°C for tumour tissue (Figure 5). At temperatures >50°C it is possible that tissues will be destroyed. These high temperatures may subsequently reduce the blood perfusion to a low rate which, at some high enough temperature, approaches zero. Under these physiological conditions, predicted tissue temperatures would be higher than those predicted in the simulations of the present study. In summary, when type, size, and site-specific (e.g. prostate, cervix, brain, etc.), temperature-dependent blood perfusion data become available, these can be used in appropriate tissue models with the numerical techniques discussed in this study.

The simulations are performed in a two-dimensional tissue model of the human prostate. Though the assumptions of long (>50 mm) thermoseeds and the use of a mid-plane cross-section satisfied modelling constraints of two-dimensional tissue models (Chen *et al.* 1991, Chin and Stauffer 1991), the complete three-dimensional aspects of this study need to be investigated. For example, Chen *et al.* (1991) have shown that two-dimensional models can significantly overestimate temperatures, and consequently, three-dimensional simulations are necessary for accurate hyperthermia treatment planning. In addition, there is some interest in the use of concurrent brachytherapy and ferromagnetic hyperthermia by combining alternately, end-to-end, short (4 mm) radiation and ferromagnetic thermoseeds in catheters (Steeves *et al.* 1989). Two-dimensional thermal models will be inadequate to determine accurate temperature distributions perpendicular to these short thermoseeds, and therefore, complete three-dimensional modelling will be necessary.

Note that using constant-rate blood perfusion models 1 and 2 underestimate the drop in $T_{max,t}$, $T_{min,t}$, and $T_{max,n}$ between simulations with constant-rate versus temperature-dependent perfusion models. That is, simulations using the highest perfusions possible in the tumour core of models 1 and 2 would produce large differences in $T_{max,t}$, $T_{min,t}$, and $T_{max,n}$ between the constant-rate and temperature-dependent models than those reported in the present study (Figures 7c and 9c).

Several environmental conditions on the outer surface of the tissue system different than those presented (Figure 4) were also investigated. Often, a patient receiving a hyperthermia treatment will be lying on their dorsal side. Under this condition, the ventral and lateral surfaces of the body will be subjected to convection heat transfer while the dorsal side contacts the treatment bed which is at room temperature. Thus additional simulations were conducted with the dorsal surface of the finite element model (lower edge in Figure 4) having a fixed-temperature (25°C) boundary condition while the upper and side surfaces had the convection boundary as discussed earlier (h=5 W/m^2/°C, T_{amb}=25°C). Temperature distributions in and near the tumour from simulations with this fixed-temperature boundary condition were identical to those obtained from simulations discussed in the present study (Figures 7–10) (unpublished data). Radiation heat transfer can also increase the rate of energy exchange between the surface of the tissue system and the surroundings. The radiation heat transfer coefficient, h_r, is computed with the relationship $h_r=\epsilon\sigma(T_{amb}^2+T_{sur}^2)(T_{amb}+T_{sur})$ (Incropera and DeWitt 1990). Here, the emissivity of skin, ϵ, can be taken as 1 and σ is the Stefan-Boltzmann constant

($=5{\cdot}67\times10^{-8}$ W/m^2/K^4). For a range of reasonable estimates for T_{amb} and T_{sur}, h_r is approximately 6 W/m^2/°C. Thus h_r is comparable in magnitude to the convection heat transfer coefficient, h. Temperature distributions in and surrounding the tumour from simulations where the heat transfer coefficient was doubled ($h=10$ W/m^2/°C) were identical to those obtained from simulations discussed in the present study (Figures 7–10) (unpublished data). The relatively large distance from the tumour site to the outer surface of the tissue system and blood perfusion at 37°C explain why temperature distributions in the tumour and local normal tissue are unaffected by any of the surface boundary conditions studied.

Simulations with constant-rate and temperature-dependent perfusion models were performed on a Macintosh IIci (Motorola 68030 processor operating at 25 MHz) and a Macintosh IIfx (Motorola 68040 processor operating at 40 MHz), respectively. Convergence of the Newton-Raphson scheme to determine all seed temperatures depended on the seed configuration. Seed combinations consisting of lower temperature seeds generally required less CPU time. CPU times were between 30 and 60 min for simulations with the constant-rate perfusion models. CPU times for simulations with the temperature-dependent perfusion models were between 3 and 5 h. Reduction in the CPU times should be possible by using faster, iterative solution schemes than the direct methods used in the present study and through dynamic allocation of computer memory. Work of this nature is in progress.

Simulations of ferromagnetic hyperthermia treatments with temperature-dependent versus constant-rate blood perfusion models reveal significant differences in temperature distributions in a model of the human prostate and surrounding normal tissues. $T_{max,t}$ is betwen 1·3 and 3·5°C lower, $T_{min,t}$ is between 1·7 and 2·6°C lower and $T_{max,n}$ is between 2·1 and 3·3°C lower with a constant-rate perfusion model versus that of a comparable temperature-dependent model. The same simulations reveal that the percentages of tumour volume at temperatures above 42°C are between 0 and 68% higher with the temperature-dependent perfusion model over all seed combinations studied. In summary, a numerical method is presented which makes it possible to investigate temperature-dependent, continuous functions of blood perfusion in simulations of hyperthermia treatments. Simulations with this numerical method reveal that the use of constant-rate instead of temperature-dependent blood perfusion models can be a conservative approach in treatment planning of ferromagnetic hyperthermia.

Acknowledgements

This work was supported in part by NIH grant CA49429.

References

ABRAMOWITZ, M. B. and STEGUN, I. A. (eds), 1964, *Handbook of mathematical functions with formulas, graphs, and mathematical tables* (New York: Dover), ch. 9.

ATKINSON, W. J., BREZOVICH, I. A. and CHAKRABORTY, D. P., 1984, Usable frequencies in hyperthermia with thermal seeds. *IEEE Transactions on Biomedical Engineering*, **31**, 70–75.

BOWMAN, H. F., 1980, Heat transfer mechanisms and thermal dosimetry. *Third International Symposium Cancer Therapy Hyperthermia, Drugs and Radiation*, Fort Collins, CO, June 22–26.

BREZOVICH, I. A., ATKINSON, W. J. and CHAKRABORTY, D. P., 1984, Temperature distributions in tumor models heated by self-regulating nickel-copper alloy thermoseeds. *Medical Physics*, **11**, 145–152.

BREZOVICH, I. A., LILLY, M. B., MEREDITH, R. F., WEPPELMANN, B., HENDERSON, R. A., BRAWNER, W. R. and SALTER, M. M., 1990, Hyperthermia of pet animal tumours with self-regulating ferromagnetic thermoseeds. *International Journal of Hyperthermia*, **6**, 117–130.

CHEN, J. S., POIRIER, D. R., DAMENTO, M. A., DEMER, L. J., BIENCANIELLOW, F. and CETAS, T. C., 1988, Development of Ni-4 weight percent Si thermoseeds for hyperthermia cancer treatment. *Journal of Biomaterials Research*, **22**, 303–319.

CHEN, Z. P., MILLER, W. H., ROEMER, R. B. and CETAS, T. C., 1990, Errors between two- and three-dimensional thermal model predictions of hyperthermia treatments. *International Journal of Hyperthermia*, **6**, 175–191.

CHEN, Z. P., ROEMER, R. B. and CETAS, T. C., 1991, Errors in the two-dimensional simulation of ferromagnetic implant hyperthermia. *International Journal of Hyperthermia*, **7**, 735–739.

CHEN, Z. P., ROEMER, R. B. and CETAS, T. C., 1992, Three-dimensional simulations of ferromagnetic implant hyperthermia. *Medical Physics*, **19**(4), 989–997.

CHIN, R. B. and STAUFFER, P. R., 1991, Treatment planning for ferromagnetic seed heating. *International Journal of Radiation Oncology, Biology and Physics*, **21**, 431–439.

CLAY ADAMS, CO., 1991, *Thermophysical properties of polyethylene tubing (PE 200)*, Clay Adams Co., Parisippany, NJ.

CLEGG, S. T. and ROEMER, R. B., 1989, Towards estimation of noisy three dimensional temperature fields during hyperthermia. *International Journal of Hyperthermia*, **5**, 467–484.

CLEGG, S. T., ROEMER, R. B. and CETAS, T. C., 1985, Estimation of complete temperature fields from measured transient temperatures. *International Journal of Hyperthermia*, **1**, 265–286.

COOPER, T. E. and TREZEK, G. J., 1971, Correlation of thermal properties of some human tissues with water content. *Aerospace Medicine*, **42**, 24–27.

DAVIES, E. J. and SIMPSON, P., 1979, *Induction heating handbook* (London: McGraw-Hill), pp. 307–340.

DEVITA, V. T., HELLMAN, S. and ROSENBERG, S. A., 1985, *Cancer: Principles and Practice of Oncology* (Philadelphia: Lippincott), pp. 932–934.

FALK, P., 1978, Patterns of vasculature in pairs of fibrosarcoma in the rat and their relation to tumor response to single large doses of radiations. *European Journal of Cancer*, **14**, 237–250.

GORDON, R. B., ROEMER, R. B. and HOWATH, S. M., 1976, A mathematical model of the human temperature regulatory system–transient cold exposure response. *IEEE Transactions on Biomedical Engineering*, **23**, 434–444.

HAIDER, S. A., CETAS, T. C., WAIT, J. R. and CHEN, J. S., 1991, Power absorption in ferromagnetic implants from radiofrequency magnetic field and the problem of optimization. *IEEE Transactions on Microwave Theory and Techniques*, **39**, 1817–1827.

HAIDER, S. A., CETAS, T. C. and ROEMER, R. B., 1993, Temperature distribution in tissues from a regular array of hot source implants: an analytical approximation. *IEEE Transactions on Biomedical Engineering*, **40**(5), 408–417.

INCROPERA, F. P. and DEWITT, D. P., 1990, *Introduction to Heat Transfer*, 2nd edn (New York: Wiley).

JAIN, R. K., 1985, Analysis of heat transfer and temperature distributions in tissues during local and whole-body hyperthermia. *Heat Transfer in Medicine and Biology*, edited by A. Shitzer and R. C. Eberhart (New York: Plenum), chapter 16.

JAIN, R. K., GRANTHAM, F. H. and GULLINO, P. M., 1979, Blood flow and heat transfer in Walker 256 mammary carcinoma. *Journal of National Cancer Institute*, **62**, 927–933.

KLEIN, S. A., BECKMAN, W. A. and MYERS, G. E., 1988–94, FEHT: Finite Element Heat Transfer software. F-chart Software, 4406 Fox Bluff Road, Middleton, WI 53562.

KOBAYASHI, T., KIDA, Y., TANAKA, T., KAGEYAMA, N., KOBAYASHI, H. and AMEMIYA, Y., 1986, Magnetic induction hyperthermia for brain tumor using ferromagnetic implant with low Curie temperature. *Journal of Neuro-Oncology*, **4**, 175–181.

LASSEN, N. A., LINDBJERG, J. and MUNCK, O., 1964, Measurement of blood flow through skeletal muscle by intra muscular injection of Xenon-133. *Lancet*, **i**, 686–689.

LIAUH, C-T., CLEGG, S. T. and ROEMER, R. B., 1991, Estimating three-dimensional temperature fields during hyperthermia: studies of the optimal regularization parameter and time sampling period. *Journal of Biomechanical Engineering*, **113**, 230–238.

LIAUH, C-T. and ROEMER, R. B., 1993a, Multiple minima in inverse hyperthermia temperature estimation problems. *Journal of Biomechanical Engineering*, **115**(3), 239–246.

LIAUH, C-T. and ROEMER, R. B., 1993b, A semilinear state and parameter estimation algorithm for inverse hyperthermia problems. *Journal of Biomechanical Engineering*, **115**(3), 257–261.

LILLY, M. B., BREZOVICH, I. A. and ATKINSON, W. J., 1985, Hyperthermia induction with thermally self-regulated ferromagnetic implants. *Radiology*, **154**, 243–244.

MATLOUBIEH, A. Y., ROEMER, R. B. and CETAS, T. C., 1984, Numerical simulation of magnetic induction heating of tumors with ferromagnetic seed implants. *IEEE Transactions On Biomedical Engineering*, **31**, 227–234.

MECHLING, J. A. and STROHBEHN, J. W., 1986, A theoretical comparison of the temperature distributions produced by three interstitial hyperthermia systems. *International Journal of Radiation Oncology, Biology and Physics*, **12**, 2137–2149.

MYERS, G. E., 1987, *Analytical Methods in Conduction Heat Transfer* (Schenectady, NY: Genium), ch. 9.

NEVINS, R. G. and DARWISH, M. A., 1970, Heat transfer through subcutaneous tissue as heat generating porous material. *Physiological and Behavioral Temperature Regulation*, edited by J. D. Hardy, A. P. Gagge, and J. A. Stolwijk (Springfield, IL: C. C. Thomas), pp. 281–301.

NIELSEN, S. L., 1972, Measurement of blood flow in adipose tissue from washout of Xenon-133 after atraumatic labelling. *Acta Physiology Scandinavia*, **84**, 187–196.

PARTINGTON, B. P., STEEVES, R. A., SU, S. L., PALIWAL, B. R., DUBIELZIG, R. R., WILSON, J. W. and BREZOVICH, I. A., 1989, Temperature distributions, microangiographic and histopathologic correlations in normal tissue heated by ferromagnetic needles. *International Journal of Hyperthermia*, **5**, 319–327.

PENNES, H. H., 1948, Analysis of tissue and arterial blood temperatures in the resting human forearm. *Journal of Applied Physiology*, **1**, 93–122.

ROEMER, R. B., 1988, Heat transfer in hyperthermia treatments: basic principles and applications. *Biological, Physical and Clinical Aspects of Hyperthermia*, edited by B. R. Paliwal, F. W. Hetzel, and M. W. Dewhirst (New York: AIP), pp. 210–242.

ROOT, W. S., 1963, The flow of blood through bones and joints. *Handbook of Physiology*, Vol. 2 (Washington, DC: American Physiological Society), Section 2, pp. 1657.

SHOUP, T. E., 1979, *A Practical Guide to Computer Methods for Engineers* (Englewood Cliffs, NJ: Prentice Hall), pp. 33–36.

SONG, C. W., LOKSHINA, A., RHEE, J. G., PATTEN, M. and LEVITT, S. H., 1984, Implication of blood flow in hyperthermic treatment of tumors. *IEEE Transactions on Biomedical Engineering*, **31**, 9–16.

STAUFFER, P. R., 1990, Techniques for interstitial hyperthermia. *Introduction to the Practical Aspects of Clinical Hyperthermia*, edited by S. B. Field, and J. W. Hand (Philadelphia, PA: Taylor & Francis), pp. 344–370.

STAUFFER, P. R., CETAS, T. C., FLETCHER, A. M., DEYOUNG, D. W., OLESON, J. R. and ROEMER, R. B., 1984a, Observations in the use of ferromagnetic implants for inducing hyperthermia. *IEEE Transactions on Biomedical Engineering*, **31**, 76–90.

STAUFFER, P. R., CETAS, T. C. and JONES, R. C., 1984b, Magnetic induction heating of ferromagnetic implants for inducing localized hyperthermia in deep-seated tumors. *IEEE Transactions on Biomedical Engineering*, **31**, 235–251.

STEEVES, R. A., PARTINGTON, B., PALIWAL, B. R. and BREZOVICH, I. A., 1989, Minimum length of ferromagnetic seeds combined with ^{125}Iodine for simultaneous interstitial hyperthermia and irradiation. *Abstracts from the 9th Annual Meeting of the North American Hyperthermia Group*, Seattle, WA, March 18–23, pp.48.

TOMPKINS, D. T., 1992, A finite element heat transfer model of ferromagnetic thermoseeds and a physiologically-based objective function for pretreatment planning of ferromagnetic hyperthermia. PhD Thesis, Department of Mechanical Engineering, University of Wisconsin-Madison, Madison, WI.

TOMPKINS, D. T., VANDERBY, R., KLEIN, S. A., BECKMAN, W. A., STEEVES, R. A. and PALIWAL, B. R., 1994, Effect of interseed spacing, tissue perfusion, thermoseed temperatures and catheters in ferromagnetic hyperthermia: results from simulations using finite element models of thermoseeds and catheters. *IEEE Transactions on Biomedical Engineering* (in press).

VANDERBY, R., PALIWAL, B. R., WAKAI, R. T., BELLOLI, D. M., PARTINGTON, B. P., STEEVES, R. A. and HEINER, J. P., 1988, A parametric study of temperature distributions in ferromagnetic hyperthermia. *Computational Methods in Bioengineering*, edited by R. L. Spilker and B. R. Simon (New York: ASME), pp. 291–299.